BioOne COMPLETE

A Class of Indices and a Graphical Tool to Monitor Temperature Anomalies

Authors: Bárcena-Martín, Elena, Molina, Julian, Hueso, Paloma, and Ruiz-Sinoga, José Damián

A Class of Indices and a Graphical Tool to Monitor Temperature Anomalies

Elena Bárcena-Martín[1], Julian Molina[2], Paloma Hueso[3] and José Damián Ruiz-Sinoga[3]

[1]Departamento de Estadística y Econometría, Universidad de Málaga, Málaga, Spain.
[2]Departamento de Economía Aplicada, Matemáticas, Universidad de Málaga, Málaga, Spain.
[3]Departamento de Geografía, Universidad de Málaga, Málaga, Spain.

ABSTRACT: We propose a graphical device—Three I's of Anomalies (TIA) curves—that provides information on the incidence, intensity, and inequality (variability) of air temperature anomalies. We also propose a class of indices that help to compare different TIA curves when visual inspection alone is inconclusive. This class of indices identifies the 3 dimensions of anomalies and can be decomposed to evaluate air temperature anomalies according to different characteristics. Moreover, the results from this class of indices are consistent with the graphical device. We calculated TIA curves and a class of indices to analyze temperature anomalies in Málaga, Spain, from 2000 to 2017. Comparison of sequential 5-year periods indicated that maximum and minimum temperature anomalies have generally increased in frequency and intensity over time. The proposed index, which considers all dimensions, indicated that maximum and minimum temperature anomalies have increased. Analysis of different geographical areas indicated that inland areas had the greatest anomalies for minimum temperatures and mountainous areas had the greatest anomalies for maximum temperatures. Inland areas also had a stronger pattern of increasing anomalies. The coastline, especially in the western region, had weaker maximum and minimum temperature anomalies.

KEYWORDS: Graphical tool, incidence of anomalies, intensity of anomalies, variability of anomalies

Introduction

Climate change is one of the greatest environmental issues facing mankind in the 21st century.[1] The continuing increases of surface temperatures worldwide are likely to cause major changes in global hydrological and energy cycles.[1] Meehl et al[2] concluded that the type, frequency, and intensity of extreme events will also change as the earth's climate changes, and these changes could occur even when there are relatively small overall mean climate changes. The increase of extreme events has manifested as an increase of droughts, heat waves, heavy precipitation, wind storms, and other events.[3,4] These extreme events continue to cause significant damage throughout the world[2,5-7] and are therefore of great concern to communities, businesses, and governments.[8,9]

Tebaldi et al[7] concluded that "the greatest threats to humans from climate change are regional changes in extreme climate events." The exact definition of an extreme event varies widely in the literature. Nonetheless, several studies during the past decade have attempted to identify previous extreme events and to project future extreme events. These studies have employed diverse temperature and precipitation data for identification of return periods[10-12]; calculation of frequency-duration-intensity indices[13]; analysis by multivariate statistics[14,15]; and development of indices based on frequency and variance.[16,17] The Intergovernmental Panel on Climate Change[18] Fourth Assessment Report (AR4) focused on 6 types of "extreme weather events" in their discussions of observed changes in extreme events and projections of future extreme events[19,20]: (1) daily maximum and minimum temperatures (coldest and hottest 10% each year); (2) heat waves; (3) heavy precipitation events; (4) droughts; (5) intense tropical cyclone activity; and (6) incidences of extreme high sea levels.

A temperature anomaly distribution describes the frequency of thermic anomalies in units of the local standard deviation.[10,21] Tebaldi et al[7] described 5 control indexes related to temperature anomalies: (1) total number of frost days, defined as the annual total number of days with an absolute minimum temperature below 0°C; (2) intra-annual extreme temperature range, defined as the difference between the highest and lowest temperature of the year; (3) growing season length, defined as the duration from the first occurrence of 5 consecutive days with mean temperature above 5°C to the last such occurrence during the year; (4) heat wave duration index, defined as the maximum period during each year in which there were at least 5 consecutive days that had maximum temperatures at least 5°C higher than the climatological norm for the same calendar days during a reference period; and (5) number of warm nights, defined as the number of times during the year when the minimum daily temperature is above the 90th percentile of the climatological distribution for that calendar day.

On a global scale, Hansen et al[21] showed that as

the global distribution of seasonal mean temperature anomalies shifted toward higher temperatures over time, the range of anomalies also increased. Quantifying and understanding temperature anomalies at the regional scale is one of the most important issues in current debates about global change.

However, there are great uncertainties about regional temperature anomalies because climate variability can mask man-made forced signals, and characterization of the natural variability is necessary to evaluate the intensity of the change in the forced signal. Many previous studies described trends and variability over a wide range of scales, from the global to the local.[6,10,21-26] The structure of climate series can differ considerably among regions and locations, and exhibit variability at different scales in response to changes in direct radiative forcing and because of variations in the internal modes of the climate system.[10,24,26,27]

In this article, we propose a graphical device that provides an intuitive understanding of air temperature anomalies that will facilitate communication with the general public and aid in advising policy makers. These graphs represent descriptive indices of the temperature anomalies most commonly analyzed: the frequency, intensity, and inequality (variability) of air temperature anomalies. Notably, comparison of 2 different distributions of anomalies can depend on the chosen dimension for analysis. To circumvent this problem, we also developed a class of indices to analyze air temperature anomalies. The proposed class of indices has important advantages. First, it can identify the relevance of all 3 major dimensions of anomalies in the air temperature distribution (frequency, intensity, and variability). Second, it is decomposable and therefore allows researchers to compare air temperature anomalies among seasons, time periods, and geographical areas. Third, its results are consistent with the proposed graphical device.

Our class of indices per se allows to track the joint evolution of the 3 dimensions of anomalies (frequency, intensity, and inequality) across time. It is attractive to analyze the evolution of each dimension separately, and indices in the literature usually focus in the frequency or/and intensity of anomalies, neglecting inequality. Our graphical device and our index also account for inequality in anomalies, a crucial feature in the climate change analysis given that we can get the same average intensity of a temperature anomaly having a quite homogeneous distribution of anomalies or with a very unequal distribution of anomalies. These 2 situations need to be treated differently and they can only be discerned with a proper measure that accounts for inequalities in anomalies.

Moreover, we can find situations in which the separate analysis of each dimensions is not conclusive and we need to aggregate the information of the 3 dimensions to have a complete picture of the situation. Our class of indices provides a consistent way to aggregate information on frequency, intensity, and inequality in anomalies. Furthermore, a graph in which the 3 dimensions are displayed is an appealing tool to communicate the results, allowing a better understanding of the change in the climate and a greater awareness of the population.

We illustrate the usefulness of the proposed class of measures of temperature anomalies by providing a detailed comparison of temperature anomalies in the province of Málaga (southern Spain) and decomposing the analysis by

5-year periods from 2000 to 2017. Our preliminary results show that our method is particularly useful in providing numerical and graphic results of temperature anomalies that have generally increased in frequency, although not in intensity, over time.

The second section of this study presents a graphical device that represents the 3 dimensions of air temperature anomalies indices. The third section introduces a class of indices that quantifies differences between profiles of air temperatures and describes their properties. The fourth section provides an empirical illustration, which shows the usefulness of our method for the numerical and graphic comparison of the frequency, severity, and variability of temperature anomalies. The last section provides a conclusion.

Graphical Tool for Analysis of Temperature Anomalies

The term *temperature anomaly* refers to a departure from a reference value or long-term average. A changing climate may lead to changes in the frequency, intensity, spatial extent, duration, and timing of temperature anomalies and may also lead to unprecedented anomalies. Because dynamical models project increases in the frequency, intensity, and duration of temperature anomalies during at least the next century,[28-30] it is important to provide definitions for temperature anomalies that are clear and commonly accepted.

The Expert Team on Climate Change Detection and Indices (ETCCDI) defined a core set of descriptive indices of temperature extremes that provide a uniform perspective of observed changes of climate extremes. These indices describe specific characteristics of extremes, some of them regarding temperature. Some indices require calculation of the number of days in a year that exceeded a specific threshold.

The 2 dimensions usually analyzed in the study of temperature anomalies are the proportion of days with a temperature anomaly (*AP*) and the average intensity of a temperature anomaly (*AI*). We define these terms formally for maximum air temperatures, but they could also be defined for minimum air temperatures. Let $Tmax \in \mathbb{R}_{++}^n$ be a vector of maximum daily temperatures and $\lambda \in \mathbb{R}_{++}^n$ be the daily threshold, let $\Gamma_i = Tmax_i - \lambda_i$ be the temperature gap of the i th day, let Q be the set of days in which $Tmax_i$ exceeds the threshold λ_i, let $q = q(Tmax, \lambda)$ be the number of days with maximum temperature anomaly, and let n be the total number of days analyzed.

Thus, the proportion of days with a *Tmax* anomaly (the *incidence* of maximum temperature anomalies, *AP*) is

$$AP = \frac{q}{n}, \tag{1}$$

and the mean maximum temperature gap per anomalous day (anomaly intensity, *AI*) is
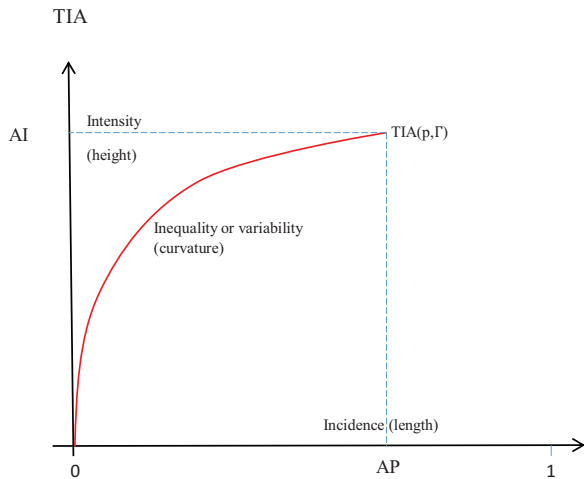
$$AI = \frac{1}{q}\sum_{i \in Q}\Gamma_i. \tag{2}$$

Figure 1. Three I's of Anomalies (TIA) curve of the 3 dimensions of temperature anomalies (incidence, intensity, and inequality).

Figure 2. Three I's of Anomalies (TIA) curves for series *a* and *b*.

We are also interested in the variability of anomalies. More variability means that anomalies are more "spread out," or equivalently that anomalies are further away from the average anomaly, showing more extreme events. One way of measuring variability is through the variance of the maximum temperature gaps (Var):

$$Var\left(\Gamma_i\right) = \frac{1}{q}\sum_{i \in Q}\left(\Gamma_i\right)^2 - \left(\frac{1}{q}\sum_{i \in Q}\Gamma_i\right)^2. \tag{3}$$

The next step is the graphical representation of these 3 aspects of temperature anomalies. This graph, which is based on temperature departure from the threshold (temperature gaps, Γ_i), depicts the visual distribution of temperature anomalies in an easily understood manner. We name this curve the *Three I's of Anomalies* (TIA) curve, which is analogous to *Three I's of Poverty* [TIP] curve in poverty analysis[31,32], because it simultaneously summarizes 3 major aspects of temperature anomalies: incidence, intensity, and inequality (variability).

The TIA curve (Figure 1) is obtained by ranking temperature gaps, $\Gamma_i = Tmax_i - \lambda_i \forall i \in Q$, in descending order (greatest gaps first), cumulating the temperature gaps per day with temperature anomaly and plotting them on a 2-dimensional graph, where we represent in the horizontal axis the cumulative proportion of days ranked in descending order of temperature gaps and in the vertical axis the running sum of Γ_i. So, values of the curve are thus defined in the interval [0, AP].

The TIA curve is denoted by TIA (p, Γ) where $0 \le p \le 1$ and p represents the cumulative proportion of anomalous days ranked in descending order of temperature gaps. Thus, the curve plots p against the sum of the first p percent Γ-values divided by the total number of days with anomalies, q, after ranking from larger to smaller temperature gaps. Then, TIA $(0, \Gamma)$ =0 and TIA $(k/n, \Gamma) = 1/q \sum_{i=1}^{k}(Tmax_i - \lambda_i)$ for integer values $k < q$, in which q is the size of the set Q, and intermediate
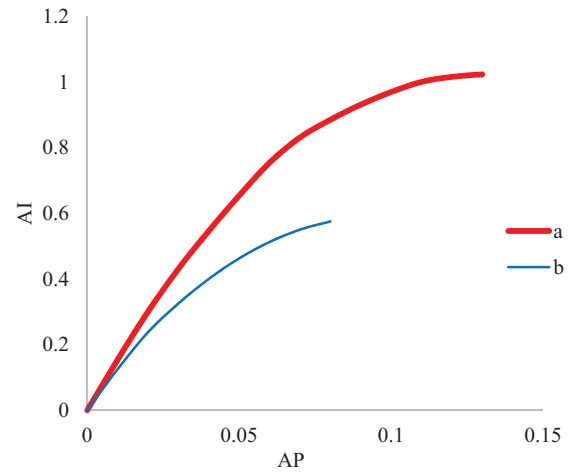
points TIA (p, Γ) are determined by linear interpolation. Therefore, TIA ($p = k/n$, Γ) is a positive, increasing and concave function of p, and the slope at each point of the curve is the mean temperature gap of the k days with greater temperature gaps.

The shape of a TIA curve provides important information about the nature of the temperature anomalies. In particular, the incidence of anomalies (proportion of days with a temperature anomaly, AP) is indicated by the value of p on the horizontal axis where the TIA curve reaches its maximum. The mean temperature gap of days with an anomaly is represented by the maximum of the TIA curve, and is a measure of the intensity of temperature anomalies. The variability in temperature anomalies is indicated by the curve's concavity. Thus, if all days with a temperature anomaly experienced the same temperature gap, the TIA curve would be a straight line with slope equal to the mean temperature gap. When temperature gaps are more unequal, the TIA curve increases in concavity.

As an illustration, consider the following 2 simulated temperature gap profiles over an observation period of 100 days ($n = 100$). The gaps in *Tmax* are

$$\Gamma^a = \{2, 1.9, 1.7, 1.5, 1.4, 1.3, 1, 0.7, 0.6, 0.5, 0.4, 0.2, 0.1\} \; and$$
$$\Gamma^b = \{1, 0.9, 0.7, 0.6, 0.5, 0.4, 0.3, 0.2\}.$$

Note that the first series has 13 days with anomalies and the second series has 8 days with anomalies. Figure 2 shows the 2 resulting TIA curves.

Series *a* has an incidence of 0.13, intensity of 1.02, and coefficient of variation (standard deviation divided by the mean) of 0.39; series *b* has an incidence of 0.08, intensity of 0.58, and coefficient of variation of 0.07. The figure clearly shows that the anomalies in profile *a* are more intense and have greater incidence and variability (indicated by greater concavity). This method allows establishment of an ordering of temperature gap profiles by nonintersecting TIA curves. Moreover, examination of these curves allows researchers to identify the
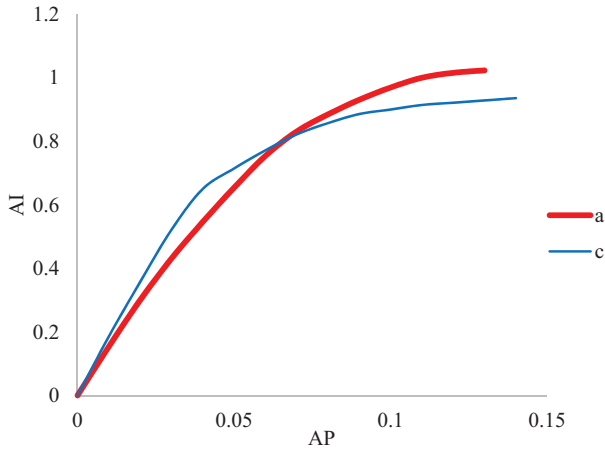
Figure 3. Three I's of Anomalies (TIA) curves for profiles *a* and *c*.

distribution of temperature gaps and to evaluate the relevance of large temperature gaps relative to medium-sized or small gaps. It is also possible to use these curves to compare temperature anomalies among different time periods, geographic regions, and any other subgroup (as shown below). This procedure also allows a definition of the concept of "dominance" in a temperature anomaly.

Definition of dominance in temperature anomaly

Given 2 relative temperature gap profiles, Γ^a and Γ^b, Γ^a dominates Γ^b in the sense of temperature anomalies, $\Gamma^a >_A \Gamma^b$, if $\Gamma^a \neq \Gamma^b$ and TIA $(p, \Gamma^a) \geqslant$ TIA (p, Γ^b) for any $p \in [0,1]$, and TIA $(p, \Gamma^a) >$ TIA (p, Γ^b) for at least one $p \in [0,1]$.

Furthermore, the TIA curve maintains its properties if truncated at low levels of anomaly for robustness (eg, excluding a gap of 0.5°C or less from analysis because of the presumably insignificant impact on well-being). The truncation point can be chosen arbitrarily. (We could have performed the same graph considering Q the set of days that belong to a heat wave, ie, the set of days in which $Tmax_i$ exceeds the threshold λ_i for at least a certain number consecutive days. This way, *AP* is the proportion of days that suffer a heat wave, and *AI* the intensity of the heat waves, ie, the mean temperature gaps per days in a heat wave. The choice of consecutive days with anomalies can be chosen arbitrarily to adapt to the definition of heat wave).

The dominance criterion is a very useful tool when comparing TIA curves that do not cross. However, consider simulated profile *c*, $\Gamma^c = \{2.6, 2.4, 2.3, 1.8, 0.9, 0.8, 0.7, 0.5, 0.4, 0.2, 0.2, 0.1, 0.1, 0.1\}$.

In this case, the incidence is 0.14, the intensity is 0.94, and the coefficient of variation is 0.81. On comparison with profile *a*, it is not immediately clear which profile is more anomalous (Figure 3). In this case, we must decide which dimension (incidence, intensity, or variability) is more important, or if we should only look at one of them.

Therefore, when TIA curves cross, or if it is necessary to quantify the differences between 2 profiles, then indices must be used to measure temperature anomalies.

Class of Air Temperature Anomaly Indices

This section describes a normative framework for the empirical study of temperature anomalies and is an adaptation of the family of poverty indices proposed by Foster et al (1984)[33]. This method provides aggregate indicators that are explicit in incorporating the necessary judgments about how to aggregate temperatures anomalies. The temperature anomaly index is based on air temperature gap, determined by the difference between the air temperature and the threshold.

Consider a maximum temperature anomaly measure, A_α, for $\alpha \geq 0$ defined by,

$$A_\alpha = \frac{1}{n}\sum_{i \in Q}\Gamma_i^{\alpha}. \qquad (4)$$

The measure of a temperature anomaly is a weighted sum of the daily temperature gap, Γ_i, in which the weight is the extent to which the temperature exceeded the threshold. Consequently, this measure gives more weight to greater temperature gaps and, as shown below, considers variability in the distribution of temperature gaps for $\alpha > 1$.

For $\alpha = 0$, the measure A_0 is the *incidence* of a maximum temperature anomaly, *AP*:

$$A_0\left(Tmax, \lambda\right) = \frac{q}{n} = AP.$$

For $\alpha = 1$, we can determine A_1 (the renormalization of the mean maximum temperature gaps):

$$A_1\left(Tmax, \lambda\right) = \frac{1}{n}\sum_{i \in Q}\Gamma_i = AP\,\frac{1}{q}\sum_{i \in Q}\Gamma_i = AP\,AI\,.$$

A_1 thus combines 2 dimensions of the anomalies—*incidence* and *intensity*. In other words, A_1 allows a ranking of the distributions of anomalies based only on these 2 dimensions.

For $\alpha = 2$,

$$A_2\left(Tmax, \lambda\right) = \frac{1}{n}\sum_{i \in Q}\Gamma_i^2.$$

Using expression (3) for the variance of the maximum temperature gaps allows determination of A_2:

$$A_2\left(Tmax, \lambda\right) = AP\,Var\left(\Gamma_i\right) + AP\left(\frac{1}{q}\sum_{i \in Q}\Gamma_i\right)^2$$
$$= AP\left[\left(Var\left(\Gamma_i\right) + AI^2\right)\right].$$

A_2 thus combines all 3 dimensions of the anomalies—*incidence*, *intensity*, and *variability*.

The parameter α can be considered a measure of aversion to higher anomalies, in that a larger α gives more emphasis to the greater anomalies. As α becomes very large, A_α tends to only consider the day with the greatest anomaly. The same reasoning can be used to develop an index of anomalies in minimum temperatures, anomalies for cooler air temperatures instead of warmer ones, or anomalies in other variables (eg, daily rain).

The class of indices proposed, A_α, has the following properties:

1. *Focus.* A_α is unaffected by *Tmax* values that do not exceed the threshold. This is apparent from the expression of the index that only accounts for anomalies.
2. *Continuity.* A_α is a continuous function. This means that small changes in an anomaly do not lead to large changes in the index.
3. *Anonymity.* This means that the index does not favor any particular anomaly in a particular day.
4. *Replication invariance.* This allows for comparisons between distributions with different sizes.
5. *Monotonicity.* This refers that an increase in the temperature of an anomalous day yields a higher index value. Therefore, *ceteris paribus*, a higher *Tmax* leads to a greater anomaly index. This property is satisfied for $\alpha \geq 1$.
6. *Effect of greater anomalies.* The allocation of an additional increase of temperature in an anomalous day increases the index more if it occurs on a day that has a greater initial anomaly.
7. *Decomposition in subgroups.* This property allows decomposition of the overall temperature anomaly index into subgroups (geographical areas, years, seasons, etc). This feature is particularly useful for identification of subgroups that have experienced more anomalies than others, so that policy makers can develop more focused interventions. This property can also be used to determine the contribution of each subgroup to the overall temperature anomaly index. Our measure of temperature anomaly has reasonable normative properties.

An Empirical Illustration: The Incidence and Intensity of Anomalies in Málaga, Spain

The Intergovernmental Panel on Climate Change (IPCC)[18] concluded that an overall increase in the number of warm days and nights on a global scale will likely occur and that anthropogenic influences will likely lead to an increase of extreme daily temperatures on a global scale. In particular, climate change has led to increased average air temperature, a change of the natural air temperature limits, and more frequent high air temperature anomalies.[34]

The report released by the IPCC in 2018,[35] Special Report on Global Warming of 1.5 degrees shows the impacts that global warming would have if exceeding pre-industrial levels by 1.5 degrees. The report warns that reducing carbon emissions will not be enough to stabilize world temperatures by 1.5 degrees; it will also require direct capture of CO_2 from the atmosphere.

This index, therefore, is a tool that lets us to address the 3 main dimensions of thermal anomalies, those related to their frequency, intensity, and variability. Furthermore, it is comparable, making it possible to determine trends between seasons, time periods, and geographic areas.

It is also a tool within the framework of Sustainable Development Goals 13,[36] since it introduces climate change as a primary issue in the policies, strategies and plans of countries, companies, and civil society, improving the response to the problems it generates and promoting education and awareness of the entire population in relation to the phenomenon.

The application of climate models to Spain offers us various projections, coinciding that the increase in maximum temperatures will have direct implications for our health, with more intense and longer heat waves, reaching over 2 weeks duration.[37]

We used daily air temperature data of 18 observatories from the Spanish meteorological agency (AEMET) to analyze maximum air temperature anomalies in the province of Málaga, in southern Spain. These data cover a variety of geographical settings (coastal, mountain, and inland regions). The air temperature data at these observatories are highly reliable for the period 1971 to 2017. Mediterranean basin ecosystems are specific climate zones that have significant interannual variability in precipitation and air temperature. Alpert et al[38] previously analyzed observational data from several areas of the Mediterranean basin using data from the 20th century and reported an increase in extreme events.

We analyzed the anomalies in daily maximum and minimum air temperatures from 2001 to 2017 and used data from 1971 to 2000 as the reference period for computation of *Tmax* and *Tmin* thresholds during the first year (2001). We then updated the reference period for subsequent years. The period of 2001 to 2017 had 105 167 daily values from 18 observatories; the period 1971 to 2000 had 186 404 daily values from the same 18 observatories.

We used a method described by Barcena-Martin et al (2019)[10] to define the daily thresholds *Tmax* and *Tmin* and to identify temperature anomalies. Below, we describe the method for computation of *Tmax; Tmin* thresholds can be computed similarly. These authors proposed calculation of a running average of the *Tmax* of a specific day with 2 adjacent days for all 30 previous calendar dates. The upper daily threshold air temperature for each day is the 95th percentile of the corresponding *Tmax* series.

Formally, $Tmax_{i,t}$ is the *Tmax* of the i Julian day of year t, and $\tilde{T}max_{i,t}$ is the *Tmax* series of the Julian day i and the 2 adjacent days ($Tmax_{i-1,t}$ $Tmax_{i+1,t}$) during the previous 30 years. Therefore,

$$\tilde{T}max_{it} = \left\{ \begin{array}{l} Tmax_{i,j}, Tmax_{i-1,j}, Tmax_{i+1,j} \, j \\ = t-30, t-29, \ldots, t-1 \end{array} \right\}.$$

We set the threshold λ_i at the 95th percentile of $\tilde{T}max_{it}$. The *Tmax* threshold in this definition depends on Julian day. This procedure filters out the effects of seasonality (obviating the need to correct values measured directly at an observatory) and year (which detrends the threshold and updates it to current conditions). Because the threshold is defined by the 30 previous calendar dates, there is not necessarily a fixed number of anomalies, because anomalies outside the period are used to compute the threshold.

These thresholds allow simple monitoring of trends in the frequency, intensity, and variability of anomalies. These
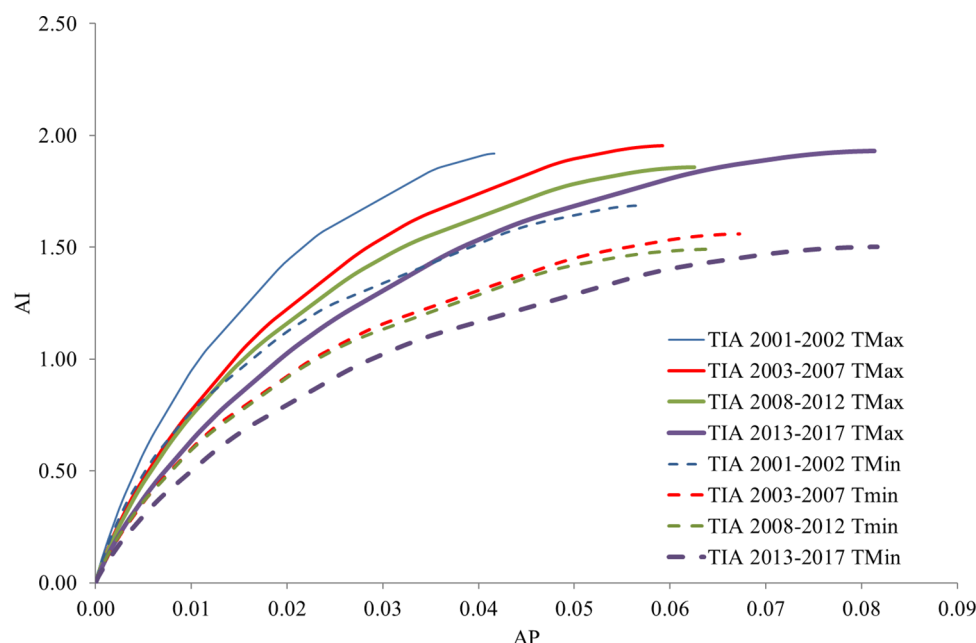
Figure 4. Three I's of Anomalies (TIA) curves for *Tmax* and *Tmin* for 5-year periods.

anomalies, even if not particularly extreme, could stress human populations or the environment.

Summing up, the daily percentile thresholds are determined empirically from the observed *Tmax* or *Tmin* series on the 30 previous calendar dates. This procedure ensures that temperature anomalies (ie, crossings of percentile thresholds) can occur with equal probability throughout the year. Thus, temperature gaps (*Tmax* or *Tmin* exceeding the percentile thresholds) are expressions of anomalies relative to the local climate. These values may provide useful (albeit indirect) information important to environmental impact studies and adaptation.

Figure 4 presents the 3 dimensions of anomalies (TIA curves) in *Tmax* and *Tmin* data. We decomposed the index into subgroups (described above) for 5-year periods.

TIA curves for later time periods end further to the right (Figure 4), except for *Tmin* 2008-2012, indicating an increasing incidence of abnormalities at *Tmax* and *Tmin*. Furthermore, the intensity of *Tmax* (maximum height of the TIA curve) decreased slightly for the subsequent time periods (except the final period, in which the intensity reached its maximum); *Tmin* intensity also decreased for later time periods (except for the last period in which the intensity was slightly higher than the previous period). These results, as demonstrated by Barcena-Martin et al[10], lead to the conclusion that temperature anomalies have generally become more frequent with time (although the intensity was less during the most recent period), except in the last period.

When ranking periods by the incidence, intensity, and variability of anomalies, rank depends on the dimension. Therefore, we can complement the TIA curves with information on indexes that combine the 3 aspects of these anomalies. We first analyzed *Tmax* and *Tmin* anomalies for the entire period (Table 1).

Table 1. Indexes for *Tmax* and *Tmin* anomalies from 2001 to 2017.

	A_0	A_1	A_2
Tmax	0.065	0.1241	0.3882
Tmin	0.070	0.1067	0.2781

These results indicate that the incidence of anomalies (ie, the proportion of anomalies, A_0) of *Tmax* was slightly lower than that of *Tmin*, which is also consistent with what was stated by Tomczyk et al (2017).[39]

However, when 2 dimensions (A_1) or the 3 dimensions of anomalies (incidence, intensity and variability, A_2) are combined, *Tmax* is more anomalous than *Tmin*, a circumstance that in our case may be due to the latitudinal factor. Division of the entire period into 5-year periods allows analysis of changes of anomalies in *Tmax* and *Tmin* over time (Table 2).

The decomposition into 5-year period shows, as in the TIA curves, that the proportion of *Tmax* and *Tmin* anomalies has increased over time, with an especially notable increase during the last period (2013-2017), which was also already reported by Chen et al (2017)[40] for China over a long period. Analysis of index A_1 and A_2, which combine dimensions of anomalies, affirms that *Tmax* had greater anomalies over time and *Tmin* had a more irregular increase of anomalies over time.

The information in Table 2 is clearly complemented by the information in Figure 4 because the TIA curves show important information that is not evident in the indices. The concavity of a TIA curve shows how temperature gaps are distributed. Our analysis allows us to compare the importance of large, medium, and small temperature gaps. For example, *Tmax* during the period from 2001 to 2002 has a strong initial increase (indicating large temperature differences); *Tmax*

Table 2. Indexes for *Tmax* and *Tmin* anomalies by 5-year periods.

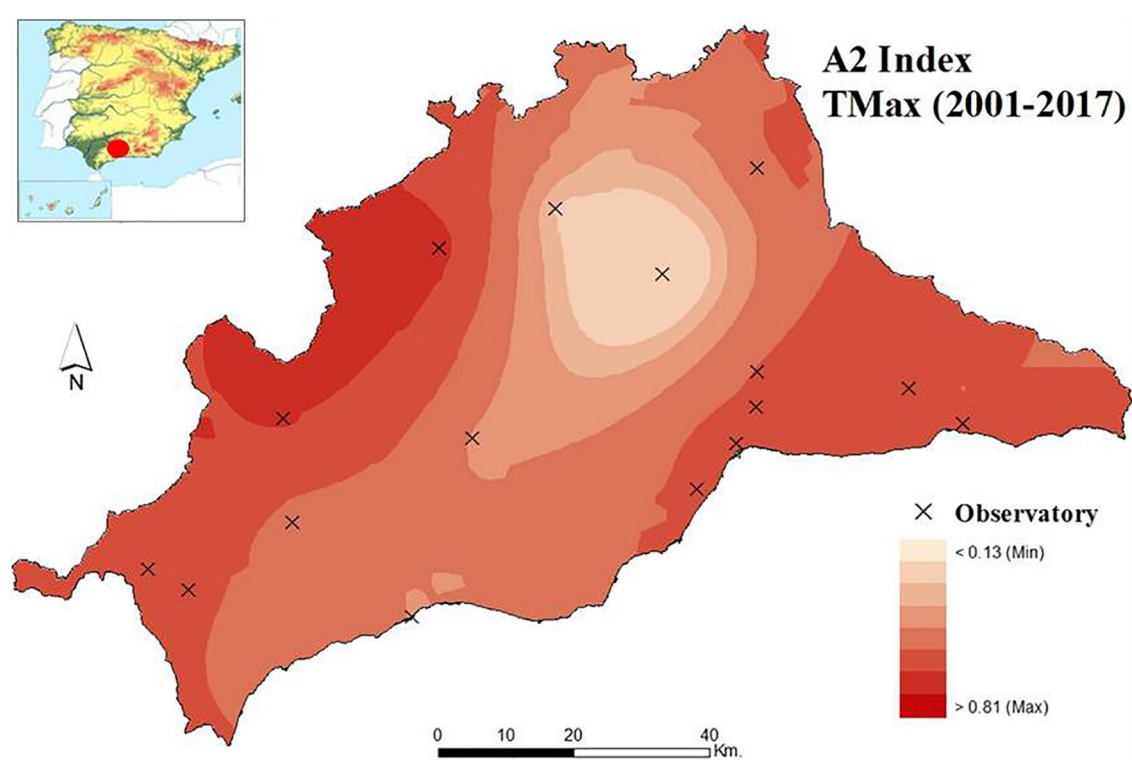|	TIME	A_0	A_1	A_2
Tmax	2001-2002	0.042	0.0799	0.2323
	2003-2007	0.059	0.1157	0.3579
	2008-2012	0.063	0.1162	0.3607
	2013-2017	0.081	0.1570	0.5047
Tmin	2001-2002	0.057	0.0956	0.2882
	2003-2007	0.067	0.1049	0.2733
	2008-2012	0.065	0.0968	0.2470
	2013-2017	0.082	0.1227	0.3104

Figure 5. Geographical distribution, using Kriging of the A_2 Index for *Tmax* anomalies, in Málaga province for the entire study period (2001-2017).

for the periods 2003 to 2007 and 2008 to 2012 had similar (but somewhat smaller) temperature gaps, as indicated by the initial overlap of these 2 curves. We consider this to be one of the greatest contributions of the TIA curves. In contrast, there were no large temperature gaps at *Tmax* for the period 2013 to 2017, but many medium-sized temperature gaps are sufficient to show the maximum incidence of the period. Our analysis of the TIAs for *Tmin* led to similar conclusions.

We also performed a geographic analysis for the province of Málaga for all 3 dimensions of anomalies (combined in the A_2 index) to show areas where the combination of incidence, intensity, and variability of anomalies was higher (Figures 5-8). Figures 5 and 6 show the values of the A_2 index for *Tmax* and *Tmin* during the entire period (2001-2017). Note that

the geographical distribution of anomalies in *Tmax* does not necessarily show greater *Tmax* values; instead, it shows *Tmax* values greater than expected given the distribution of daily *Tmax* during the past 30 years (Figure 5). A similar interpretation applies to the geographical distribution of anomalies in *Tmin* (Figure 6).

The province of Malaga, due to its geographical characteristics, located at the western Mediterranean Sea and in the southernmost part of Spain, south of the Baetic mountain ranges, is suffering various effects closely related to the new climatic pattern. Its proximity to the Atlantic Ocean through the Strait of Gibraltar gives it a certain trait of oceanity, in such a way that it marks an incidence of the longitudinal pluviometric gradient, tending toward aridity as moving to the east. But
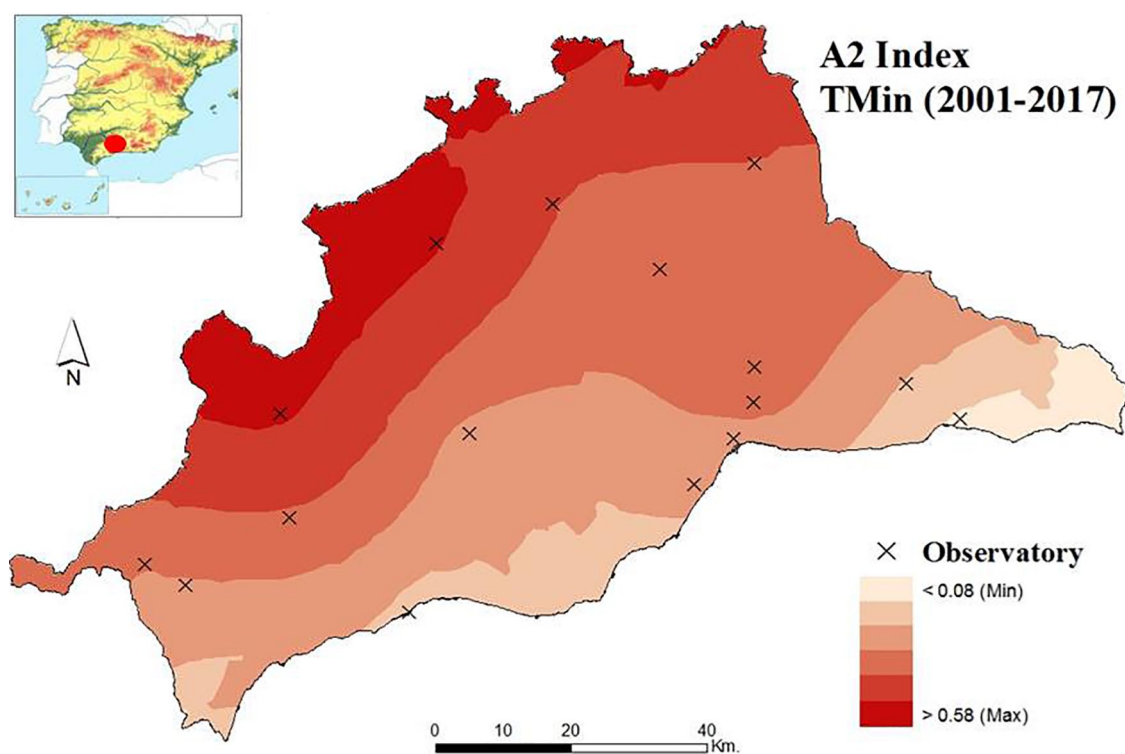
Figure 6. Geographical distribution, using Kriging of the A_2 Index for *Tmin* anomalies, in Málaga province for the entire study period (2001-2017).
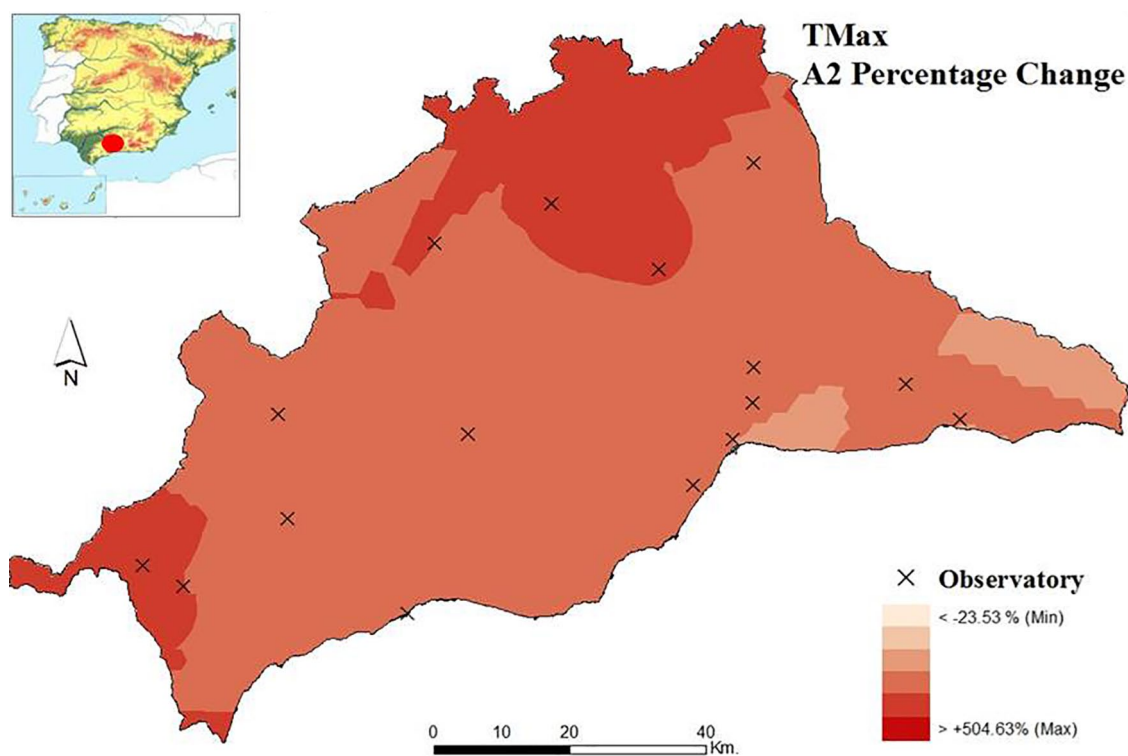

Figure 7. Geographical distribution, using Kriging of the A_2 Index, for the difference of *Tmax* from 2013 to 2017 relative to 2003 to 2007.

its longitudinal arrangement is joined by the presence of an intricate orography, with a whole series of mountain ranges that rush from north to south toward the Mediterranean, but which also protect it from the dreaded north winds.

All this endows it with a singular climatic dynamic, and especially significant in the last decades. Proximity to the ocean has been translated into a double pluviometric pattern, with a divergent trend toward higher humidity in the
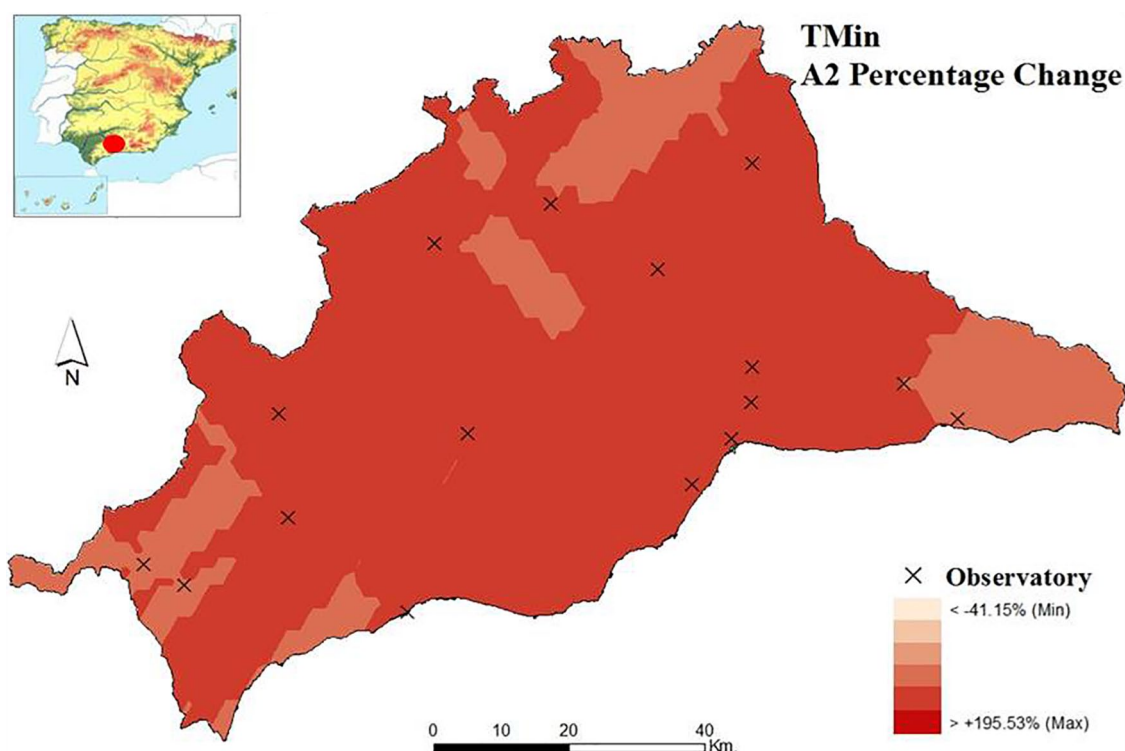
Figure 8. Geographical distribution, using Kriging of the A_2 Index, for the difference of *Tmin* from 2013 to 2017 relative to 2003 to 2007.

western zone and toward greater aridity from the center to the east.[41] This modification of the pluviometric pattern has resulted, on the one hand, in a greater succession of droughts and dry spells, attending to this pattern along the pluviometric gradient[42,43] and, on the other hand, in a higher frequency of torrentiality, generating serious territorial consequences.[44,45]

These modifications in the climatic pattern have also affected the thermal dynamics of the area, manifested in a greater succession of heat waves,[10] and thus having as a reference the period 1970-2000, has been verified both the proliferation of heat waves in all the years from 2001 to 2016, some even reaching a significant number (20 in 2015), and the circumstance of not only having heat waves during the summer periods, as, in fact, months with more heat waves were May and October.

The results, after the application of the proposed index, show that the greatest anomalies in *Tmax* (Figure 5) are found mainly in the mountainous areas (northwest), and the interior region has fewer anomalies. In contrast, the *Tmin* anomalies (Figure 6) mostly have a latitudinal pattern, with an increase from the coast to the more inland regions.

That is, they are the areas with the greatest temperature anomalies: inland for *Tmin* and mountainous areas for *Tmax* (Figures 5 and 6). Coastal regions, especially in the west, have apparently had less extreme maximum and minimum temperature anomalies.

The territorial representation of the percentage change for *Tmax* and *Tmin* between 2003 and 2017 shows that the region furthest from the coast had the greatest changes in *Tmax* over

time (Figure 7). Furthermore, considering Figures 5 and 7 together shows that the northwest region had the least pronounced anomalies (A_2) (Figure 5) and the largest increase in anomalies over time.

The *Tmin* analysis (Figure 8) indicates a mostly uniform pattern throughout Malaga, although the incidence of anomalies was lower in the mountainous areas (east, west, and some inland areas).

In short, the changes in the climatic pattern, also manifested by a greater succession of heat waves, follow an uneven spatial pattern. And thus, the greatest anomalies, the most frequent, intense and variable, are found in the interior areas, while in the coastal areas, the effect of the sea's thermal smoothing attenuates them. This is especially evident in the maximum temperatures, which follow a clear pattern of continentality, while the minimum temperatures tend to be more uniform, because of the regulatory role of the Mediterranean.

Conclusions

1. The proposed index identifies the relevance of thermal anomalies in their incidence, intensity, and inequality, being able to be comparable in different seasons, time periods, geographic areas and according to the graphic device.
2. It is effective in representing noticeable changes in maximum and minimum temperature anomalies over time.
3. In southern Spain, in particular, these anomalies have increased in frequency, with a variable intensity, except during the last 5 years, in which there is a clear increase in both intensity and frequency.

4. *Tmax* has steadily increased anomalies throughout the period considered, while *Tmin* had major and irregular anomalies only at the end of the period.

5. In geographical terms, the distribution of thermal anomalies in Malaga seems to have a unique pattern. The inland region (for maximum and minimum temperatures) and the mountainous areas (for maximum temperatures) had the greatest temperature anomalies, being the coast, due to the smoothing effect of the sea, the least anomalous area.

Acknowledgements

Author Contributions

All authors have contributed equally to the research.

ORCID iD

José Damián Ruiz-Sinoga   https://orcid.org/0000-0002-2303-0881

REFERENCES

1. Houghton JT, Ding Y, Griggs DJ, et al. Climate *Change* 2001: *The Scientific Basis. Contribution of Working Group* I to the *Third Assessment Report of the Intergovernmental Panel on Climate Change*. Cambridge, UK; New York, NY: Cambridge University Press; 2001.

2. Meehl GA, Karl T, Easterling DR, et al. An introduction to trends in extreme weather and climate events: Observations, socioeconomic impacts, terrestrial ecological impacts, and model projections. *B Am Meteorol Soc*. 2000;81:413-416. doi:10.1175/1520-0477(2000)081<0413.

3. Schär C, Vidale PL, Lüthi D, et al. The role of increasing temperature variability in European summer heatwaves. *Nature*. 2004;427:332-336. doi:10.1038/nature02300.

4. Beniston M, Stephenson DB, Christensen OB, et al. Future extreme events in European climate: An exploration of regional climate model projections. *Climatic Change*. 2007;81:71-95. doi:10.1007/s10584-006.

5. Kunkel KE, Pielke RA, Changnon SA. Temporal fluctuations in weather and climate extremes that cause economic and human health impacts: A review. *B Am Meteorol Soc*. 1999;80:1077-1098.

6. Easterling DR, Meehl GA, Parmesan C, Changnon SA, Karl TR, Mearns LO. Climate extremes: Observations, modeling, and impacts. *Science*. 2000;289:2068-2074. doi:10.1126/science.289.5487.2068.

7. Tebaldi C, Hayhoe K, Arblaster JM, Meehl GA. Going to the extremes: An intercomparison of model-simulated historical and future changes in extreme events. *Climatic Change*. 2006;79:185-211. doi:10.1007/s10584-006.

8. Katz R, Brush G, Parlange M. Statistics of extremes: Modeling ecological disturbances. *Ecology*. 2005;86:1124-1134. doi:10.1890/04-0606.

9. Negri DH, Gollehon NR, Aillery MP. The effects of climatic variability on US irrigation adoption. *Climatic Change*. 2005;69:299-323.

10. Barcena-Martin E, Molina J, Ruiz- Sinoga JD. Issues and challenges in defining a heat wave: A Mediterranean case study. *Int J Climatol*. 2019;39:331-342. doi:10.1002/joc.5809.

11. Ekstrom M, Fowler H, Kilsby C, Jones PD. New estimates of future changes in extreme rainfall across the UK using regional climate model integrations. 2. Future estimates and use in impact studies. *J Hydrol*. 2005;300:234-251. doi:10.1016/j.jhydrol.2004.06.019.

12. Semmler T, Jacob D. Modeling extreme precipitation events a climate change simulation for Europe. *Global Planet Change*. 2004;44:119-127. doi:10.1016/j.gloplacha.2004.06.008.

13. Khaliq MN, St- Hilaire A, Ouarda T, Bobee B. Frequency analysis and temporal pattern of occurrences of southern Quebec heatwaves. *Int J Climatol*. 2005;25:485-504. doi:10.1002/joc.1141.

14. Bohm U, Kucken M, Hauffe D, Gerstengarbe F, Werner P. Reliability of regional climate model simulations of extremes and of long-term climate. *Nat Haz Earth Syst Sci*. 2004;4:417-431.

15. Huth R, Pokorna L. Simultaneous analysis of climatic trends in multiple variables: An example of application of multivariate statistical methods. *Int J Climatol*. 2005;25:469-484. doi:10.1002/joc.1146.

16. Palmer TN, Ralsanen J. Quantifying the risk of extreme seasonal precipitation events in a changing climate. *Nature*. 2002;415:512-514. doi:10.1038/415512a.

17. Meehl GA, Tebaldi C. More intense, more frequent, and longer lasting heat waves in the 21st century. *Science*. 2004;305:994-997. doi:10.1126/science.1098704.

18. Field CB, Barros V, Stocker TF, et al. *Climate Change 2012: Managing the Risks of Extreme Events and Disasters to Advance Climate Change Adaptation. A Special Report of Working Groups I and II of the Intergovernmental Panel on Climate Change*. Cambridge, UK; New York, NY: Cambridge University Press; 2012.

19. Solomon S, Qin D, Manning M, et al. *Climate Change 2007: The Scientific Basis, Contribution of Working Group I to the Fourth Assessment Report of the IPCC*. Cambridge, UK: Cambridge University Press; 2007.

20. Parry M, Canziani O, Palutikof J, van der Linden P, Hanson C. *Climate Change 2007: Impacts, adaptation, and vulnerability, contribution of Working Group II to the Fourth Assessment Report of the IPCC*. Cambridge, UK: Cambridge University Press; 2007.

21. Hansen J, Ruedy R, Sato M, Lo K. Global warming continues. *Science*. 2002;295:275. doi:10.1126/science.295.5553.275c.

22. Nicholls N, Gruza GV, Jouzel J, Karl TR, Ogallo LA, Parker DE. Observed climate variability and change. In: Houghton JT, Meira Filho LG, Callander BA, Harris N, Kattenberg A, Maskell K, eds. *Climate Change 1995; The Science of Climate Change, Ch 3. Contribution of Working Group I to the Second Assessment Report of the Intergovernmental Panel on Climate Change (IPCC)*. Cambridge, UK: Cambridge University Press; 1994:133-192.

23. Jones PD. Hemispheric surface air temperature variations: A reanalysis and update to 1993. *J Climate*. 1994;7:1794-1802.

24. Hansen J, Ruedy R, Sato M, et al. A closer look at United States and global surface temperature change. *J Geophys Res*. 2001;106:947-923. doi:10.1029/2001JD000354.

25. Folland CK, Karl TP, Christy JR, et al. Observed climate variability and change. In: Houghton JT, Ding Y, Griggs DJ, Noguer M, Van Der Linden PJ, Xiaoxu D, eds. Climate Change 2001; *The* Scientific Basis, Ch 2. Contribution of Working Group I to the Third Assessment Report of the Intergovernmental Panel on Climate Change (IPCC). Cambridge, UK: Cambridge University Press; 2001:99-181.

26. New MG, Hulme M, Jones PD. Representing twentieth-century space time climate variability. Part I: Development of a 1961–1990 mean monthly terrestrial climatology. *J Climate*. 1999;12:829-856. doi:10.1175/1520-0442(1999)012<0829:RTCSTC>2.0.CO;2.

27. Giorgi F. Variability and trends of sub-continental scale surface climate in the twentieth century. Part I: Observations. *Clim Dyn*. 2002;18:675-691. doi:10.1007/s00382-001-0204-x.

28. Kharin VV, Zwiers FW, Zhang X, Hegerl GC. Changes in temperature and precipitation extremes in the IPCC ensemble of global coupled model simulations. *J Climate*. 2007;20:1419-1444. doi:10.1175/JCLI4066.1.

29. Fischer EM, Schär C. Consistent geographical patterns of changes in high-impact European heatwaves. *Nat Geosci*. 2010;3:398-403. doi:doi.org/10.1038/ngeo866.

30. Perkins SE, Alexander LV, Nairn JR. Increasing frequency, intensity and duration of observed global heatwaves and warm spells. *Geophys Res Lett*. 2012;39:1-5. doi:10.1029/2012GL053361.

31. Jenkins SP, Lambert PJ. Three I's of poverty curves, with an analysis of UK poverty trends. *Oxford EP*. 1997;49:317-327. doi:10.1093/oxfordjournals.oep.a028611.

32. Jenkins SP, Lambert PJ. Three I's of poverty curves and poverty dominance: TIPs for poverty analysis. *Res Ec Ineq*. 1998;49:39-56.

33. Foster JE, Greer J, Thorbecke E. A class of decomposable poverty measures. *Econometrica*. 1984;52:761-766.

34. Trenberth KE, Meehl J, Masters J, Somerville R. Heat waves and climate change. A science update from climate communication. https://www.climatecommunication.org/new/features/heat-waves-and-climate-change/overview/. Updated 2012.

35. Masson-delmotte V, Zhai P, Pörtner H-O, et al. Summary for policymakers. In: Masson-delmotte V, Zhai P, Pörtner H-O, et al., eds. *Global Warming of 1.5°C. An IPCC Special Report on the Impacts of Global Warming of 1.5°C Above Pre-industrial Levels and Related Global Greenhouse Gas Emission Pathways, in the Context of Strengthening the Global Response to the Threat of Climate Change, Sustainable Development, and Efforts to Eradicate Poverty*. Geneva: IPCC; 2018:1-24.

36. United Nations Sustainable Development Goals Knowledge platform. Transforming our world: The 2030 agenda for sustainable development. https://sustainabledevelopment.un.org/post2015/transformingourworld.

37. Morata Gasca A. *Guía de escenarios regionalizados de cambio climático sobre España a partir de los resultados del IPCC-AR4* (NIPO: 281-14-002-7). Madrid, Spain: Ministerio de Agricultura, Alimentación y Medio Ambiente Agencia Estatal de Meteorología; 2014:202.

38. Alpert P, Ben-Gai T, Bahard A, et al. The paradoxical increase of Mediterranean extreme daily rainfall in spite of decrease in total values. *Geophys Res Lett*. 2002;29:1536. doi:10.1029/2001GL013554.

39. Tomczyk AM, Półrolniczak M, Bednorz E. Circulation conditions' effect on the occurrence of heat waves in western and southwestern Europe. *Atmosphere*. 2017;8:31. doi:10.3390/atmos8020031.

40. Chen Y, Hu Q, Yang Y, Qian W. Anomaly based analysis of extreme heat waves in eastern China during 1981–2013. *Int J Climatol*. 2017;37:509-523. doi:10.1002/joc.4724.

41. Ruiz-Sinoga JD, Garcia Marin R, Martinez-Murillo JF, Gabarron Galeote MA. Precipitation dynamics in southern Spain: Trends and cycles. *Int J Climatol*. 2010;30: 2281-2289. doi:10.1002/joc.2235.

42. Ruiz-Sinoga JD, Garcia-Marin R, Gabarron-Galeote MA, Martinez-Murillo JF. Analysis of dry periods along a pluviometric gradient in Mediterranean southern Spain. *Int J Climatol*. 2012;32:1558-1571. doi:10.1002/joc.2376.

43. Ruiz Sinoga JD, León Gross T. Droughts and their social perception in the mass media (southern Spain). *Int J Climatol*. 2013;33:1556. doi:10.1002/joc.3465.

44. Senciales Gonzalez JM, Ruiz-Sinoga JD. Análisis espacio-temporal de las lluvias torrenciales en la ciudad de Málaga. *B Asoc Geogr Esp*. 2013;61:15-33. doi:10.21138/bage.1533.

45. Sillero-Medina JA, Hueso-González P, Ruiz-Sinoga JD. La precipitación geomorfológica como elemento clave en el modelado del paisaje mediterráneo. *B Asoc Geogr Esp*. 2019;82:1-40. doi:10.21138/bage.2780.